Fully Printed Flexible Fingerprint-like Three-Axis Tactile and Slip Force and Temperature Sensors for Artificial Skin

Shingo Harada, Kenichiro Kanao, Yuki Yamamoto, Takayuki Arie, Seiji Akita, and Kuniharu Takei*

Department of Physics and Electronics, Osaka Prefecture University, Sakai, Osaka 599-8531, Japan

ABSTRACT A three-axis tactile force sensor that determines the touch and slip/friction force may advance artificial skin and robotic applications by fully imitating human skin. The ability to detect slip/friction and tactile forces simultaneously allows unknown objects to be held in robotic applications. However, the functionalities of flexible devices have been limited to a tactile force in one direction due to difficulties fabricating devices on flexible substrates. Here we demonstrate a fully printed fingerprint-like three-axis tactile force and temperature sensor for artificial skin applications. To achieve economic macroscale devices, these sensors are fabricated and integrated using only printing methods. Strain engineering enables the strain distribution to be detected upon applying a slip/friction force. By reading the strain difference at four integrated force sensors for a pixel, both the tactile and slip/friction forces can be analyzed simultaneously. As a proof of concept, the high sensitivity and selectivity for both force and temperature are demonstrated using a 3 × 3 array artificial skin that senses tactile, slip/friction, and temperature. Multifunctional sensing components for a flexible device are important advances for both practical applications and basic research in flexible electronics.

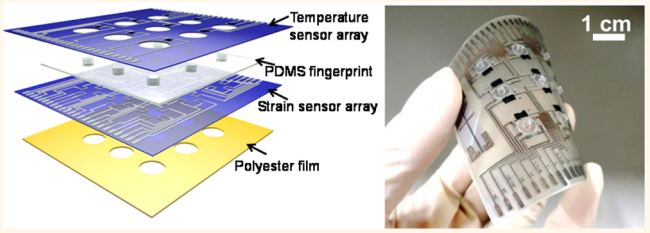

KEYWORDS: artificial skins · three-axis tactile sensors · temperature sensors · printed sensors · nanotubes · nanoparticles

Artificial electronic skins (e-skins) have been widely developed using organic[1−4] and inorganic materials[5−10] as a force and/or temperature[2,11] sensor to mimic human skin. Structural engineering realizes a highly sensitive force sensor with mechanical flexibility. Previous studies have mainly focused on materials and fabrication techniques to form tactile force sensors[3,4,6,7,9,10] and/or transistors[1,2,5,8] on a mechanically flexible substrate. To mimic the full functionality of human skin in robotic and prosthesis applications, slip (or friction) is also important information to grab an object.

A human detects tactile and slip forces simultaneously when holding an object without breaking or dropping it.[12,13] If the slip is not detected, an unknown object cannot be held. However, slip force sensor has yet to be demonstrated for an e-skin due to difficulties realizing multifunctional sensing on a flexible substrate. In addition to detecting forces, the human skin can detect temperature upon touching an object or by air flow (wind). E-skin should have similar capabilities.

To apply this kind of macroscale device to various applications, the fabrication process must be economical. However, flexible devices, including previously reported e-skins, often use semiconductor infrastructures such as lithography and vacuum systems,[1−10] except for a few demonstrations (*e.g.*, an ultraviolet photodetector using printable ZnO nanowires[14] and transistors[15,16]). Considering the device size (macroscale) and costs, a different infrastructure may be more feasible. If such a macroscale multifunctional flexible device can be realized, the technology can also be applied to different flexible and wearable electronics without employing semiconductor processes.[17−19]

In this study, we propose a strain-engineered three-axis tactile force sensor and temperature sensor array to address simultaneously the slip force, tactile force, and temperature using a macroscale printing fabrication technique. Although strain[20,21] and temperature[22] sensors have been developed using inorganic and organic materials, the material composition ratio as the printed inks is optimized for three-axis tactile force

* Address correspondence to takei@pe.osakafu-u.ac.jp.

Received for review November 4, 2014 and accepted December 1, 2014.

Published online December 01, 2014
10.1021/nn506293y

detection as explained in detail later in this report. It is noteworthy that the proposed method does not use a vacuum deposition system or optical lithography for metal and sensor formation and patterning. The sensors can be formed by a printing method (*e.g.*, screen printing on a flexible substrate). This work demonstrates highly integrated printed sensors with multifunctionality on a flexible substrate. This integration and strain engineering using a *fingerprint*-like structure allows tactile and slip forces to be detected similar to human skin. This demonstration should be important not only for e-skin and robotic applications but also for diverse multifunctional printed flexible electronic applications such as smart walls and wearable devices.

RESULTS AND DISCUSSION

To detect the three-axis force directions, four strain sensors printed by a screen printer were designed with a fingerprint-like structure fabricated by polydimethylsiloxane (PDMS). Here, a fingerprint-like structure used in this study is a three-dimensional prong with 2 mm diameter and 1 mm height, as shown in Figure 1b, that can create strain distribution by applying three-axis forces on a prong. Figure 1a shows the layer-by-layer device structure (see Methods and Supporting Information). Each layer consists of a strain sensor array, temperature sensor array, and fingerprint-like structure. After lamination, the 3 × 3 array device can detect the three-axis force (*i.e.*, tactile force and slip force) and the temperature distribution similar to a human skin. Figures 1c, S1, and S2 show more details of the fabrication process and images of each layer. Figure 1d and e exhibit the final device structure with mechanically flexible integrated three-axis force and temperature sensor arrays. Both sensors indicate the electrical resistance changes as functions of strain and temperature (Figure 1f and g).

First, the structural changes with an emphasis on the strain distributions were characterized by the finite element method (FEM) when the force was applied from the top or side of the fingerprint-like structure. Figure 2a indicates the structural changes for different applied force directions simulated by two-dimensional FEM. Applying force from the top of the structure (F_z) uniformly depresses the membrane with the strain sensors (Figure 2a left), resulting in identical strain distributions for each sensor. On the other hand,

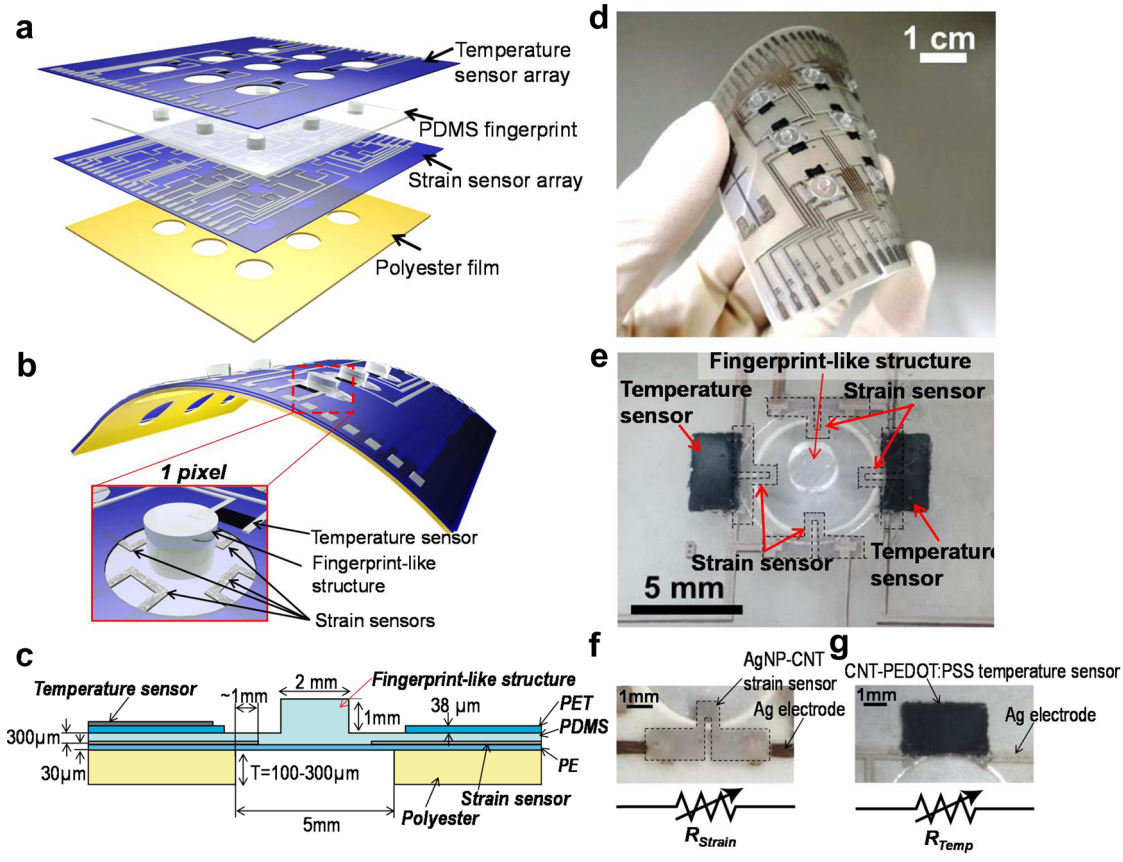

Figure 1. e-skin device with fingerprint-like structures. (a) Schematic for each layer of the e-skin device. (b) Schematic of the final e-skin device and an enlarged pixel with a fingerprint-like structure containing four strain sensors and a temperature sensor. (c) Cross-sectional schematic of the device structure with dimensions. (d) Picture of a 3 × 3 array e-skin. Enlarged pictures of (e) a pixel, (f) a strain sensor consisting of a printed AgNP-CNT film and a Ag electrode, and (g) a temperature sensor consisting of a printed CNT-PEDOT:PSS and a Ag electrode.

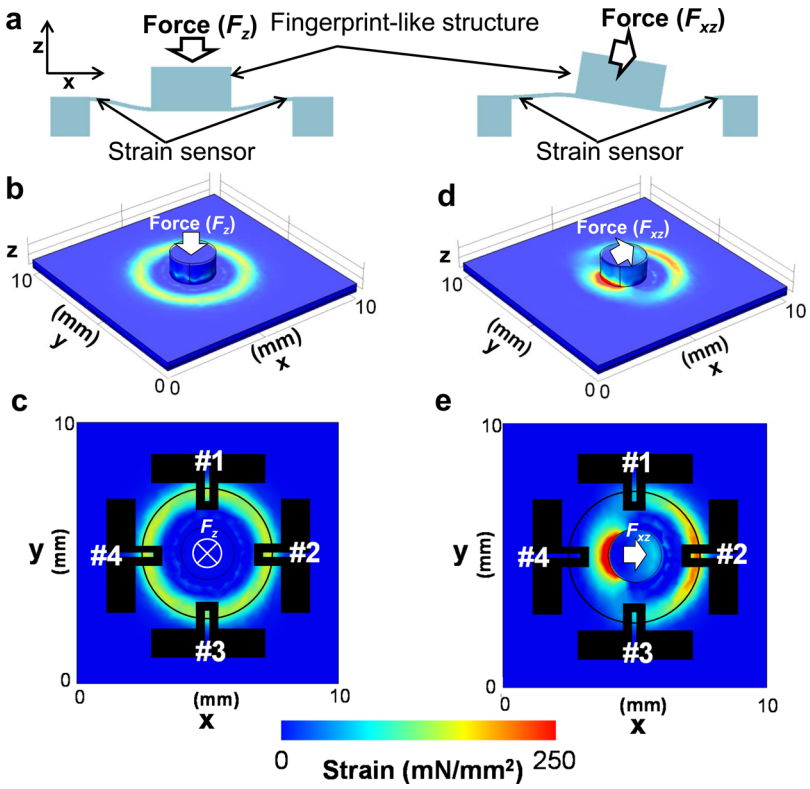

Figure 2. FEM simulations to realize three-axis force detection. (a) Structural difference simulated by FEM when F_z (touch) and F_{xz} (slip/friction) forces are applied. Three-dimensional FEM results when F_z (10 mN) is applied viewed (b) at a tilt and (c) from the top, demonstrating a uniform strain distribution at the four strain sensors. Three-dimensional FEM results when F_{xz} (F_x = 10 mN and F_z = 5 mN) is applied viewed (d) at a tilt and (e) from the top, showing that the strain distribution at the four strain sensors is not uniform. This nonuniformity allows the device to detect slip.

applying a force from the top left (F_{xz}) to create a slip/friction force (Figure 2a right) results in a completely different situation. The left side of the membrane is raised, while the right side is depressed. Placing the four strain sensors on the membrane as shown in Figure 1e can monitor the change in strain. Consequently, the strength of F_{xz} can be calculated by reading the outputs of the four strain sensors.

To confirm that the strength of F_{xz} can be calculated, the three-dimensional simulated strain distribution was mapped out using FEM. Figure 2b and c show the stress distribution when F_z is applied. As expected, the stress distribution in the strain sensors is the same as the maximum tensile stress of 15.3 mN/mm^2 at an applied force of 10 mN. On the other hand, when F_{xz} (F_x = 10 mN and F_z = 5 mN) is applied, the stress distribution of the two strain sensors along the *x*-axis differs (Figure 2d and e). It should be noted that both strain sensors have tensile stress because the PE substrate is slightly stretched upon applying force. The tensile stress is larger than the compressive stress due to bending the membrane up. Although both strain sensors have tensile stress, the strength of the stress differs. Thus, the slip direction and strength can be readily calculated *via* the difference in the resistance of the two sensors.

To confirm the stress/strain distribution difference when F_x and F_{xz} are applied, electrical measurements were experimentally carried out. First, the dependence of the strain sensor on polyester thickness was characterized as a function of applied force (Figure 3a). Figure 3b shows the normalized resistance change, $\Delta R(=R - R_0)/R_0$, where R_0 and R are the electrical resistances of the strain sensor in the flat state and under an applied force, respectively. The applied force was measured by a force sensor (LVS-50GA, KYOWA, Japan). The normalized resistance changes linearly as a function of the applied force until the bottom of the PE substrate touches the stage. According to the linear fit, the extracted force sensitivity is ~1%/mN. After the membrane touches the stage, further stress/strain cannot be applied; hence, the resistance of the strain sensor becomes constant. The trend of the resistance change (linear and saturated regions) agrees well with the FEM simulated displacement due to an applied force. Changing the polyester thickness can protect the device from breaking if the applied force is too high as well as tune the force dynamic range. On the basis of the FEM simulations, the tensile stress is equal when the force, F_z, is applied (Figure 2b and c). Real-time measurements of the four strain sensors (Figure 3c) suggest that every strain sensor detects the same force when an 11 mN force (F_z) is applied onto the fingerprint-like structure. It is noteworthy that the output force is calibrated by the results in Figure 3b.

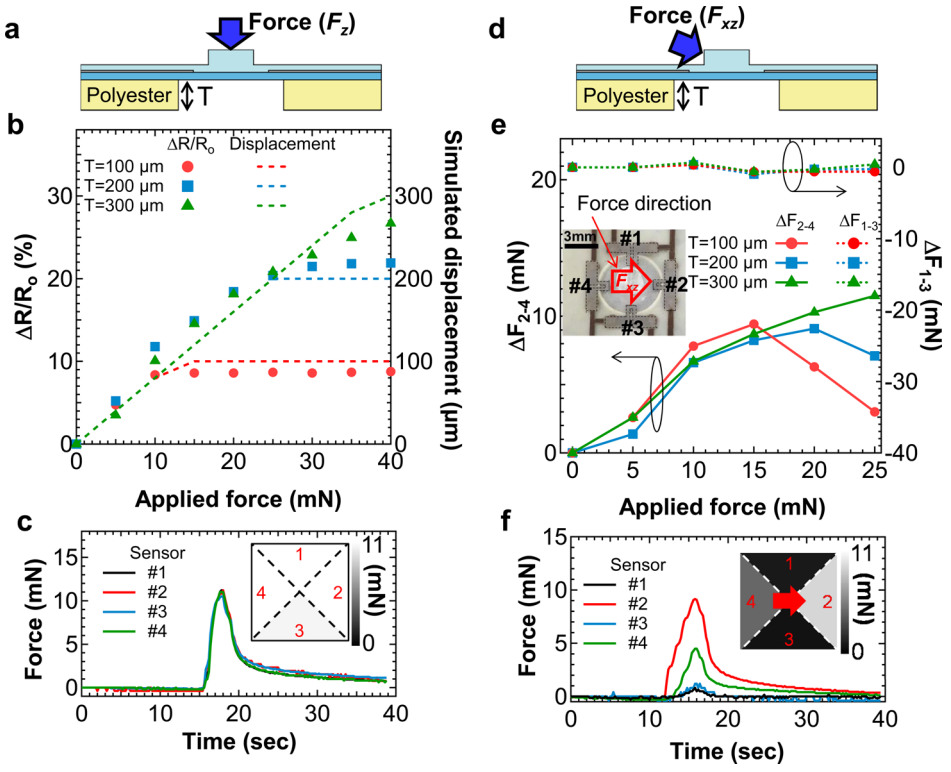

Figure 3. Electrical characteristics of the strain sensor. (a) Schematic and (b) normalized resistance change, $\Delta R/R_0$, and simulated membrane displacement as a function of an applied force of F_z with various polyester thicknesses. (c) Real-time force detection of the four strain sensors in a pixel when F_z is applied as only a tactile force (*i.e.*, touch) onto a fingerprint-like structure. (d) Schematic and (e) force difference of ΔF_{2-4} and ΔF_{1-3} extracted from strain sensors #2 and #4 and strain sensors #1 and #3, respectively, as a function of an applied force of F_{xz} with various polyester thicknesses. (f) Real-time force detection of the four strain sensors in a pixel when F_{xz} is applied as touch and slip/friction similar to human skin onto a fingerprint-like structure.

Figure S3 shows more details for four-sensor detection in a pixel as a function of polyester thickness.

Next the slip detection was demonstrated by applying the force, F_{xz} (Figure 3d). Additionally, the influence of polyester thickness (100 to 300 μm) was evaluated. According to the FEM simulations, when the force is applied from the #4 strain sensor to the #2 strain sensor (Figure 3e inset), the #2 strain sensor has a higher tensile strain than #4, but the #1 and #3 sensors have similar tensile strains. To consider this stress/strain difference, Figure 3e plots the measured force difference, $\Delta F_{2-4} = F_2 - F_4$ and $\Delta F_{1-3} = F_1 - F_3$, as a function of the applied force, where F_m (m = 1, 2, 3, 4) is the detected force of each strain sensor. The numbers (1−4) correspond to the sensor numbers in the inset of Figure 3e. The force difference, ΔF_{2-4}, gradually increases as the applied force increases, but the force difference, ΔF_{2-4}, starts to decrease at a point that depends on the polyester thickness (Figure 3e). This decrease is because the membrane deformation is too large and the membrane on strain sensor #2 touches the stage, preventing a further increase for sensor #2, whereas the strain in sensor #4 can still increase (Figure S4). This observation clearly indicates that the properties depend on polyester thickness (Figures 3e and S4). The force difference, ΔF_{2-4}, between sensors #2 and #4 is caused by stress difference in the sensors when the slip force, F_{xz}, is applied because the slip force creates nonuniform stress along sensors #2 and #4. More details of the force difference of each sensor are shown in Figure S4. In fact, experimental results indicate a similar trend of the stress distribution estimated by FEM simulation as shown in Figure 2e. On the other hand, the stress distribution in sensors #1 and #3 is identical, resulting in the strain sensor indicating the same resistance change (Figure S4). This results in $\Delta F_{1-3} \approx 0$. On the basis of these experiment and simulated trends of measured force difference, it can estimate the applied slip force and direction. As described in the FEM simulation (Figure 2d and e), it is confirmed experimentally that ΔF_{1-3} is almost 0 mN regardless of the applied force and the polyester thickness. Real-time measurements of the detected force from the four strain sensors in a pixel clearly depend on the force direction (Figure 3f). When ~8 mN (F_x) and a few mN (F_z) force is applied on the side of the fingerprint-like structure, each strain sensor has different outputs (~9, ~4.5, ~1, and ~1 mN for sensors #2, #4, #1, and #3, respectively). It should be noted that since an only one-directional force detector was used in this experiment, the force could not be measured in the z-direction (*i.e.*, F_z). Reading the strain sensor

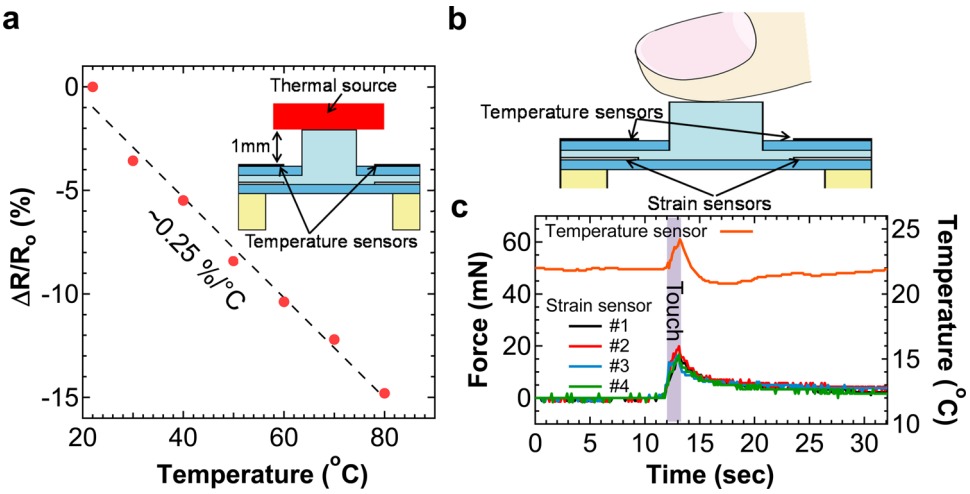

Figure 4. Electrical characteristics of an integrated temperature sensor. (a) Normalized resistance change, $\Delta R/R_0$, as a function of temperature up to 80 °C. Linear fit suggests the sensitivity is ~0.25%/°C. Inset depicts the experimental setup used to characterize the temperature sensor. Temperature sensor is not directly in contact with the thermal source. (b) Schematic and (c) results of real-time measurements of the temperature and strain sensors upon touching a fingerprint-like structure with a human finger (F_z).

output difference along the *x*- and *z*-directions can estimate the force direction corresponding to the slip force.

For e-skin applications to completely mimic human skin, temperature sensing is another key function. The temperature sensor sheet was placed on a strain sensor sheet. Due to the height (1 mm) of the fingerprint-like structure, the temperature sensor does not directly come into contact with an object (Figure 4a inset). To simulate a real situation, the temperature sensor was characterized as a function of temperature using the setup in Figure 4a inset. Figure 4a indicates the normalized resistance difference, $\Delta R(=R - R_0)/R_0$, as a function of temperature between 21 and 80 °C, where R_0 and R are the resistances at 21 °C and the set temperature up to 80 °C, respectively. The temperature sensitivity extracted from the linear fit in Figure 4a is ~0.25%/°C. Real-time simultaneous measurements of the strain and temperature sensors are also conducted by touching the device with a human finger (Figure 4b). The temperature along with the response time of <1 s or ~2 s can be measured when a finger touches or is removed from the device, respectively. This slow response is due to the low thermal conductivity of PDMS (~0.15 W/mK), PET (~0.24 W/mK), PE (~0.33 W/mK), and polyester (~0.05 W/mK) because the temperature sensor and heat source (*i.e.*, finger) are not in direct contact.

As a fully operational e-skin demonstration, a 3 × 3 array of the strain and temperature sensors was tested by touching the device with a human finger. N_2 gas flow detection was also conducted because human skin can feel moving air (wind) without touching physically. Because each pixel has four strain sensors and one temperature sensor, 36 strain sensors and nine temperature sensors were integrated on a flexible substrate *via* a printing technique only. The device was connected to a multimemory recorder (HIOKI, Japan) *via* a flexible printed circuit (FPC) board (Figure 5a and 5b).

To demonstrate that a three-axis tactile force sensor array can be integrated on a flexible substrate using a printing technique, Figure 5c and d show the tactile force (F_z) and temperature distributions, respectively. The force and temperature are clearly mapped. There is a small force difference in a pixel because the object is a human finger, which has difficulty applying the only F_z force precisely. It should be noted that the temperature sensor of pixel #2 in Figure 5c can also detect the temperature change due to proximity temperature detection (*i.e.*, radiation heat) from human skin because the temperature sensor is highly sensitive. Subsequently, a finger generates a friction force (*i.e.*, F_{xz}) (Figure 5e and f). The results indicate that the friction force distribution in an array can be successfully monitored.

Next N_2 gas with a source pressure of ~0.2 MPa flowed to the device by controlling the flow direction from pixels #2 to #8 (Figure 5g). The gas flow rate at pixel #2 was around 15.5 m/s. The temperature difference between where the device was measured (room temperature ~21 °C) and N_2 gas (~17 °C) shows the temperature distribution corresponds to the N_2 flow distribution. On the basis of the results in Figure 5g, N_2 gas is spread further from the source of N_2, which agrees well with the nature of gas/wind flow. More importantly, the strain sensors do not show any force detection due to low N_2 flow pressure, suggesting that the device can distinguish between a touch and wind flow similar to human skin. This demonstration confirms that the printable e-skin can mimic the full functionality of human skin.

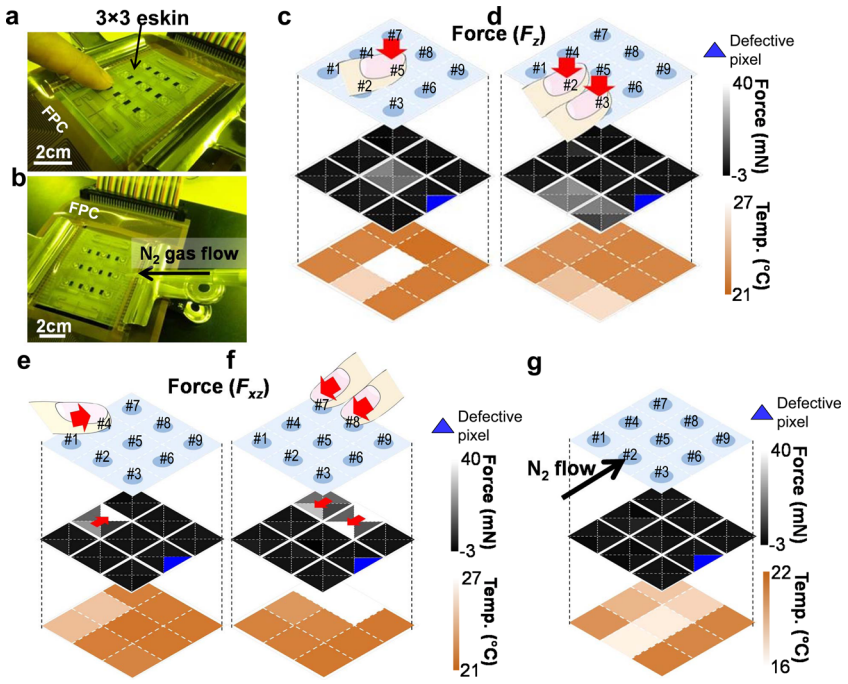

Figure 5. Demonstrations of a 3 ×3 array e-skin. Pictures of the experimental setup when (a) force is applied by a human finger and (b) N_2 gas is applied without touching the e-skin. Two-dimensional force and temperature mappings when touch, F_z, is applied onto (c) pixel #5 by a finger and (d) pixels #2 and #3 by two fingers. Two-dimensional mappings when slip/touch, F_{xz}, is applied onto (e) pixel #4 by a finger and (f) pixels #7 and #8 by two fingers. (g) Two-dimensional force and temperature mappings with a N_2 gas flow (N_2 source pressure of ~0.2 MPa and 15.5 m/s at the point of sensor #2).

CONCLUSIONS

In summary, we developed a three-axis force sensor and a temperature sensor on a flexible substrate using a printing method through stress/strain engineering. The fingerprint-like structure allows the device to detect the three-axis force for tactile and slip measurements by developing a fingerprint-like structure. In addition, the device integrates a temperature sensor array to demonstrate a fully functional e-skin application that imitates human skin. Because each pixel has four strain sensors and one temperature sensor, a total of 45 sensors are integrated on a flexible substrate in the 3 × 3 pixel array using only a printing technique. Although only a 3 × 3 pixel array on a 8 × 8 cm^2 substrate that has much lower resolution and smaller size than those of human skin was demonstrated in this study as a proof of concept, it is mostly possible to scale up and realize high resolution by using an automatic printing method, which is well controlled for applied pressure and speed for printing. In fact, for example, the technology to make a screen-print mask with 3 micrometer resolution on a macroscale substrate (813 × 711 mm^2) is commercially available from Screen Holdings Co., Ltd., in Japan. By using the mask and an optimized ink and a condition of printing such as pressure, speed, and angle of a squeegee, the e-skin can be scaled up with high-resolution pixels (*e.g.*, at least 10 μm resolution and ±5 μm alignment accuracy) in the future. As we demonstrated the integration of sensors, it is possible to integrate different components if the active material inks such as sensors, transistors, and actuators are developed. This technique, which prepares highly integrated printable sensors, will be applicable not only to e-skins but also to a variety of future flexible and wearable electronics that require economic macroscale fabrication processes and high performances.

METHODS

Silver Electrode Printing. A silver (Ag) electrode was printed by a screen printing method using commercially available Ag ink (Asahi Chem., Japan) on a 30 μm thick polyethylene (PE) and a 38 μmn thick polyethylene terephthalate (PET) film as a strain sensor array and a temperature sensor array at a curing temperature of 70 and 130 °C, respectively.

Strain Sensor Printing. A mixture of carbon nanotube (CNT) ink (SWeNT, USA) and Ag nanoparticle (AgNP) ink (Paru, Korea) with a weight ratio of 5:3 was printed with the alignment of the Ag interconnection. The alignment accuracy and resolution of printed patterning were around ±10 μm for both the *x*- and *y*-axes and about 200 μm for line patterning, respectively. To observe the three-axis force, a membrane structure with the strain sensors was created by laminating a polyester film with 5 mm diameter holes under the strain sensors. Subsequently, the fingerprint-like PDMS structure with a 2 mm diameter and 1 mm height was attached in the center of the membrane (Figure 1b).

Temperature Sensor Printing. The temperature sensor was printed using a mixture ink of CNT ink (SWeNT, USA) and conductive poly(3,4-ethylenedioxythiophene)-poly(styrenesulfonate)

(PEDOT:PSS, 1.3 wt % in water) (Sigma-Aldrich, USA) with a weight ratio of 1:3 *via* a shadow mask printing method. Both sensor materials were cured at 70 °C. To laminate with the strain sensor sheet, 6 mm diameter holes in the temperature sensor array sheet were created by a laser cutter tool.

Layer Lamination. To laminate all layers to assemble the e-skin, first, a polyester film with one-side adhesion (Nitto Denko, 3198MS sheet, Japan) was attached on the bottom of the strain sensor sheet. The fingerprint-like structure made of PDMS was placed onto the strain sensor sheet using a molecule gradient layer tape (KGK, Japan). Finally, the temperature sensor sheet was attached onto the PDMS fingerprint-like structure without any adhesive due to the stickiness between PDMS and PET.

Electrical Measurement. Each strain sensor and temperature sensor was connected to a commercially available multichannel data logger (Hioki, Japan) to directly measure the resistance of every sensor. The sampling rate of data recording was 100 ms.

Conflict of Interest: The authors declare no competing financial interest.

Acknowledgment. This work was partially supported by JSPS Kakenhi grants (#26630164 and #26709026), the Mazda Foundation, and Tateishi Science and Technology Foundation.

Supporting Information Available: Details of the fabrication process and electrical characteristics of four strain sensors on a pixel upon applying tactile and slip forces. These materials are available free of charge *via* the Internet at http://pubs.acs.org.

REFERENCES AND NOTES

1. Someya, T.; Sekitani, T.; Iba, S.; Kato, Y.; Kawaguchi, H.; Sakurai, T. A Large-Area, Flexible Pressure Sensor Matrix with Organic Field-Effect Transistors for Artificial Skin Applications. *Proc. Natl. Acad. Sci. U.S.A.* **2004**, *101*, 9966–9970.
2. Someya, T.; Kato, Y.; Sekitani, T.; Iba, S.; Noguchi, Y.; Murase, Y.; Kawaguchi, H.; Sakurai, T. Conformable, Flexible, Large-Area Networks of Pressure and Thermal Sensors with Organic Transistor Active Matrixes. *Proc. Natl. Acad. Sci. U.S.A.* **2005**, *102*, 12321–12325.
3. Schwartz, G.; Tee, B. C.-K.; Mei, J.; Appleton, A. L.; Kim, D. H.; Wang, H.; Bao, Z. Flexible Polymer Transistors with High Pressure Sensitivity for Application in Electronic Skin and Health Monitoring. *Nat. Commun.* **2013**, *4*, 1859.
4. Hammock, M. L.; Chortos, A.; Tee, B. C.-K.; Tok, J. B.-H.; Bao, Z. The Evolution of Electronic Skin (E-Skin): A Brief History, Design Considerations, and Recent Progress. *Adv. Mater.* **2013**, *25*, 5997–6038.
5. Takei, K.; Takahashi, T.; Ho, J. C.; Ko, H.; Gillies, A. G.; Leu, P. W.; Fearing, R. S.; Javey, A. Nanowire Active-Matrix Circuitry for Low-Voltage Macroscale Artificial Skin. *Nat. Mater.* **2010**, *9*, 821–826.
6. Kim, D.-H.; Lu, N.; Ma, R.; Kim, Y.-S.; Kim, R.-H.; Wang, S.; Wu, J.; Won, S. M.; Tao, H.; Islam, A.; *et al*. Epidermal Electronics. *Science* **2011**, *333*, 838–843.
7. Wu, W.; Wen, X.; Wang, Z. L. Taxel-Addressable Matrix of Vertical-Nanowire Piezotronic Transistors for Active and Adaptive Tactile Imaging. *Science* **2013**, *340*, 952–957.
8. Wang, C.; Hwang, D.; Yu, Z.; Takei, K.; Park, J.; Chen, T.; Ma, B.; Javey, A. User-Interactive Electronic Skin for Instantaneous Pressure Visualization. *Nat. Mater.* **2013**, *12*, 899–904.
9. Park, J.; Lee, Y.; Hong, J.; Ha, M.; Jung, Y.-D.; Lim, H.; Kim, S. Y.; Ko, H. Giant Tunneling Piezoresistance of Composite Elastomers with Interlocked Microdome Arrays for Ultrasensitive and Multimodal Electronic Skins. *ACS Nano* **2014**, *8*, 4689–4697.
10. Pang, C.; Lee, G.-Y.; Kim, T.-i.; Kim, S. M.; Kim, H. N.; Ahn, S.-H.; Suh, K.-Y. A Flexible and Highly Sensitive Strain-Gauge Sensor Using Reversible Interlocking of Nanofibres. *Nat. Mater.* **2012**, *11*, 795–801.
11. Webb, R. C.; Bonifas, A. P.; Behnaz, A.; Zhang, Y.; Yu, K. J.; Cheng, H.; Shi, M.; Bian, Z.; Liu, Z.; Kim, Y.-S.; *et al*. Ultrathin Conformal Devices for Precise and Continuous Thermal Characterization of Human Skin. *Nat. Mater.* **2013**, *12*, 938–944.
12. Johansson, R. S.; Westling, G. Roles of Glabrous Skin Receptors and Sensorimotor Memory in Automatic Control of Precision Grip When Lifting Rougher or More Slippery Objects. *Exp. Brain Res.* **1984**, *56*, 550–564.
13. Johansson, R. S.; Westling, G. Signals in Tactile Afferents from the Fingers Eliciting Adaptive Motor Responses during Precision Grip. *Exp. Brain Res.* **1987**, *66*, 141–154.
14. Liu, X.; Gu, L.; Zhang, Q.; Wu, J.; Long, Y.; Fan, Z. All-Printable Band-Edge Modulated ZnO Nanowire Photodetectors with Ultra-High Detectivity. *Nat. Commun.* **2014**, *5*, 4007.
15. Lau, P. H.; Takei, K.; Wang, C.; Ju, Y.; Kim, J.; Yu, Z.; Takahashi, T.; Cho, G.; Javey Fully Printed, High Performance Carbon Nanotube Thin-Film Transistors on Flexible Substrates. A. *Nano Lett.* **2013**, *13*, 3864–3869.
16. Jung, M.; Kim, J.; Noh, J.; Lim, N.; Lim, C.; Lee, G.; Kim, J.; Kang, H.; Jung, K.; Leonard, A. D.; *et al*. All-Printed and Roll-to-Roll-Printable 13.56-MHz-Operated 1-bit RF Tag on Plastic Foils. *IEEE Trans. Electron Devices* **2010**, *57*, 571–580.
17. Jang, K.-I.; Han, S. Y.; Xu, S.; Mathewson, K. E.; Zhang, Y.; Jeong, J.-W.; Kim, G.-T.; Webb, R. C.; Lee, J. W.; Dawidczyk, T. J.; *et al*. Rugged and Breathable Formss of Stretchable Electronics with Adherent Composite Substrates for Transcutaneous Monitoring. *Nat. Commun.* **2014**, *5*, 4779.
18. Son, D.; Lee, J.; Qiao, S.; Ghaffari, R.; Kim, J.; Lee, J. E.; Song, C.; Kim, S. J.; Lee, D. J.; Jun, S. W.; *et al*. Multifunctional Wearable Devices for Diagnosis and Therapy of Movement Disorders. *Nat. Nanotechnol.* **2014**, *9*, 397–404.
19. McAlpine, M. C.; Ahmad, H.; Wang, D.; Heath, J. R. Highly Ordered Nanowire Arrays on Plastic Substrates for Ultrasensitive Flexible Chemical Sensors. *Nat. Mater.* **2007**, *6*, 379–384.
20. Takei, K.; Yu, Z.; Zheng, M.; Ota, H.; Takahashi, T.; Javey, A. Highly-Sensitive Electronic-Whiskers Based on Patterned Carbon Nanotube and Silver Nanoparticle Composite Films. *Proc. Natl. Acad. Sci. U.S.A.* **2014**, *111*, 1703–1707.
21. Harada, S.; Honda, W.; Arie, T.; Akita, S.; Takei, K. Fully Printed, Highly Sensitive Multifunctional Artificial Electronic Whisker Arrays Integrated with Strain and Temperature Sensors. *ACS Nano* **2014**, *8*, 3921–3927.
22. Honda, W.; Harada, S.; Arie, T.; Akita, S.; Takei, K. Human-Interactive, Health-Monitoring Wireless Devices Fabricated by Macroscale Printing Techniques. *Adv. Funct. Mater.* **2014**, *24*, 3299–3304.